SynRM Sensorless Torque Estimation Using High Frequency Signal Injection

Maria Martinez, Diego F. Laborda, David Reigosa, Daniel Fernandez, J.M. Guerrero, and Fernando Briz
Department of Electrical Engineering, University of Oviedo, 33204 Gijón, Spain
martinezgmaria@uniovi.es, dflaborda@uniovi.es, diazdavid@uniovi.es, fernandezalodaniel@uniovi.es,
guerrero@uniovi.es, fernando@isa.uniovi.es

***Abstract*—Precise output torque control is often required in applications using synchronous reluctance machines. Direct measurement of torque has drawbacks due to both cost and reliability issues. To overcome these limitations, the development of torque estimation methods has received significant research attention. Most of the exiting torque estimation methods require knowledge of machine parameters, suffering therefore from parameter sensitivity. Load and saturation are recognized as the primary source of parameter variation. This paper proposes the use of high frequency signal injection for on-line estimation of the machine parameters required for torque estimation. The improvement in the torque estimation will be especially relevant in deep-saturation regions. The method operates without interfering with the normal operation of the machine.**

***Index Terms*–High frequency signal injection, synchronous reluctance machines, online parameter estimation, torque estimation.**

I. Introduction

Synchronous reluctance machines (SynRM) are characterized by their high tolerance to over-currents and/or overheating, and overall increased robustness compared with other types of ac machines such as Permanent Magnet Synchronous Machines (PMSMs) or Induction Motors (IMs), resulting from the absence of brushes, permanent magnets, or coils in the rotor. Compared with PMSMs, SynRMs have a robuster structure which facilities their use in harsh ambient, and are also more cost effective [1]–[3]. Compared with IMs, the absence of cage winding results into a reduction of the rotor losses and a lighter structure which improves their dynamic behaviour. These characteristics make them a promising alternative for high-performance applications, like traction applications up to low-speed high-power machines or industrial tools [2]. However, their high non-linear behaviour resulting from saturation results in large variation of the inductances with the operating conditions [3]–[6]. Consequently, torque control based on the mathematical modeling of the machine will be drastically affected in terms of precision and dynamics [3], [6]–[13].

Many high-performance applications, such as robotics, machine tools and EV/HEVs applications require precise control of the output torque produced by the machine [1], [3], [6]. Thus, torque measurement or estimation is therefore required. [8]–[12]. Rotary torque transducers based on strain gauges are likely the preferred option for the first case [14]–[19]. However, this type of sensors could introduce resonances into the system and require precise mounting and calibration to ensure accurate measurements [20]. Alternatively, torque can be measured using systems based on torsional displacement measurement [21], systems based on magneto-elastic effect [22] or systems based on Giant Magnetoresistive (GMR) effect [23]. However, regardless of the method being used, precise torque measurement is expensive, and requires extra elements (sensor, cables, connectors, ...), that could reduce the reliability and increase the overall cost of the drive. As an alternative, torque can be estimated.

Torque estimation methods can be roughly divided into two main groups: those based on the General Torque Equation (GTE) [8], [9], [24], [25] and indirect estimation methods [12], [13], [24], [26], [26]–[38]. Indirect estimation methods include electric power and shaft speed measurement based method [26]; flux observers based methods [12], [13], [24], [26]–[38] and optimal recursive estimation algorithms [12]. Most of the torque estimation methods reported in the literature [12], [13], [24]–[43] require precise knowledge of machine parameters (e.g. resistances or inductances). Consequently, parameter variation with the operating conditions (i.e. saturation level, temperature) can lead to large torque estimation errors, saturation being the main concern for SynRM. Look-up-tables (LUTs) are frequently used for online machine parameter adaptation [25], [42]; unfortunately, LUTs fail in the event of any type of machine degradation, and often require large memory usage.

To overcome LUTs limitations, on-line parameter estimation methods have been proposed [44]–[46]. Injection of a High-Frequency (HF) signal into the stator terminals of the machine has been reported to be a viable option for on-line machine parameter estimation. These methods can operate in the whole speed range, including zero speed, and without interfering with the normal operation of the machine.

However, HF injection based parameters estimation methods proposed so far [42], [44]–[46] typically make two assumptions: 1) machine is assumed to have a purely inductive behaviour and 2) the relationship between the high-frequency

This work was funded in part by the Research, Technological Development and Innovation Programs of the Spanish Ministry Economy and Competitiveness of the Spanish Government under the project MINECO-17-ENE2016-80047-R, in part by the Government of the Principality of Asturias under grant Severo Ochoa PA-20-PF-BP19-010 and the project IDI/2018/000188, by the University of Oviedo under grant PAPI 2018-PF-12 and in part by grants of the European Regional Development Fund (ERDF)

parameters and the fundamental parameters are assumed to be linear. While these assumptions can be acceptable for PMSMs, they can be problematic for the case of SynRMs [3], [47], [48].

This paper proposes a new on-line machine parameter estimation method, aimed to enhance torque estimation based on GTE for SynRMs. The parameters involved in the GTE are estimated from the machine reaction to a HF signal injected in the stator terminals. The proposed method shares some similarities with [44], where two pulsating HF currents were used to estimate the machine parameters; two HF current controllers being therefore required to inject the two pulsating HF currents. In this paper, machine parameters will be estimated from the injection of a single rotating HF voltage signal. Reducing the injected signals from two HF currents to one HF voltage will reduce the adverse effects due to the HF signals and simplify the implementation of the method. Additionally, a detailed study of the relationship between the HF parameters and fundamental parameters (i.e. those involved in the torque equation) will be presented. An accurate modeling of this relationship will be key to improve the torque estimation accuracy in the whole operating range of the machine. The proposed method can be used in the whole speed operating range of the machine, including stand still, eliminating therefore the need of additional controllers that are traditionally used to enable smooth transition between current to voltage based models in flux observed based torque estimation techniques [33], [42].

The paper is organized as follows: fundamental model of a SynRM is presented in section II; parameter estimation using rotating voltage HF signal is presented in section III; torque estimation based on the GTE using the estimated HF parameters is presented in section IV; simulation results obtained by means of Finite Element Analysis (FEA) are shown in section V ; implementation of the method and experimental results are presented in section VI and conclusions are finally provided in section VII.

II. Fundamental Model of a SynRM

The fundamental model of a SynRM in a reference frame synchronous with the rotor is given by (1)-(2) [3], [5], [6]:

$$v_{sd}^r = R_d\ i_{sd}^r + \frac{d\lambda_{sd}^r}{dt} - \omega_r\ \lambda_{sq}^r \tag{1}$$

$$v_{sq}^r = R_q\ i_{sq}^r + \frac{d\lambda_{sq}^r}{dt} + \omega_r\ \lambda_{sd}^r \tag{2}$$

where R_d, R_q, are the dq-axes resistances, i_{sd}^r, i_{sq}^r are the dq-axes stator currents, v_{sd}^r, v_{sq}^r are the dq stator voltages, λ_{sd}^r and λ_{sd}^r are dq-axes stator flux linkages and ω_r is the mechanical rotational speed.

The output torque is defined as:

$$T_e = \frac{3}{2}P\ (\lambda_{sd}^r\ i_{sq}^r - \lambda_{sq}^r\ i_{sd}^r) \tag{3}$$

Equation (3) can be also expressed as a function of the stator inductances (also known as apparent inductances) (5), the torque being (4). It is noted that T_e defined in (4) stands for the mean output torque of the machine.

It can be observed from (4) that the reluctance torque production by a SynRM depends on the saliency effect, i.e. it is proportional to the difference between d- and q-axes inductances.

$$T_e = \frac{3}{2}P\left((L_d - L_q)\ i_{sd}^r\ i_{sq}^r\right) \tag{4}$$

$$L = \frac{\lambda}{i} = \frac{N^2\mu_s(H)A}{l} \tag{5}$$

where i is the current, λ is the resulting flux linkage, N is the number of turns of the stator winding, μ_s is the static permeability of the material, A is the mean cross-sectional area of the magnetic circuit and l is the mean length of the magnetic circuit. The static permeability defined in (5) is defined as the ratio of flux density (B) vs. field intensity (H). As the relationship between B and H for ferromagnetic materials is usually non-linear, the static permeability is not constant but a non-linear function of H [49]–[51].

It is noted therefore that dq-axes inductances values can change with the machine operating point (6)-(7) .

$$L_{d(I_{sd},I_{sq})} = L_{d0}\left(1 + \alpha_{I_{sdd}(I_{sd},I_{sq})}I_{sd}^r + \alpha_{I_{sdq}(I_{sd},I_{sq})}I_{sq}^r\right) \tag{6}$$

$$L_{q(I_{sd},I_{sq})} = L_{q0}\left(1 + \alpha_{I_{sqd}(I_{sd},I_{sq})}I_{sd}^r + \alpha_{I_{sqq}(I_{sd},I_{sq})}I_{sq}^r\right) \tag{7}$$

where L_{d0} and L_{q0} are the dq-axes synchronous inductances when there is no dq fundamental current injection; I_{sd}^r and I_{sq}^r are the fundamental dq-axes stator current magnitude; $\alpha_{I_{sdd}(I_{sd},I_{sq})}$ and $\alpha_{I_{sdq}(I_{sd},I_{sq})}$ are the coefficients linking the d-axis inductance with the d-axis fundamental current (I_{sd}^r) due to saturation and q-axis fundamental current (I_{sq}^r) due to cross-coupling, respectively; similarly, $\alpha_{I_{sqq}(I_{sd},I_{sq})}$ and $\alpha_{I_{sqd}(I_{sd},I_{sq})}$, are the coefficients linking the q-axis inductance with the q-axis fundamental current (I_{sq}^r) due to saturation and d-axis fundamental current (I_{sd}^r) due to cross-coupling, respectively.

Substituting (6) and (7) into (4), the GTE can be written as (8).

$$T_{e_{(I_{sd},I_{sq})}} = \frac{3P}{2}\left(\left(L_{d(I_{sd},I_{sq})} - L_{q(I_{sd},I_{sq})}\right)\ i_{sd}^r\ i_{sq}^r\right) \tag{8}$$

It has to be noted that the variation of inductances with load, (6)-(7), will depend on machine design, different functions could be used to model this behavior, e.g. linear, quadratic or higher order polynomials. A commissioning process would be therefore required to obtain the required coefficients [3].

III. Parameter Estimation Using Rotating HF Voltage Injection

Machine parameters can be estimated in real time from the machine response to a small HF signal which is added on top of the fundamental voltage applied for torque production.

This section describes the physical principles of dq-axes HF inductances estimation using this method.

The HF model representing the behaviour of a synchronous machine (9) can be deduced from the corresponding fundamental frequency model (1)-(2) [52], [53].

$$\begin{bmatrix} v^r_{sdHF} \\ v^r_{sqHF} \end{bmatrix} = \begin{bmatrix} R_{dHF} + pL_{dHF} & -\omega_r L_{qHF} \\ \omega_r L_{dHF} & R_{qHF} + pL_{qHF} \end{bmatrix} \begin{bmatrix} i^r_{sdHF} \\ i^r_{sqHF} \end{bmatrix} \tag{9}$$

where

v^r_{sdHF} : d-axis HF voltage in the rotor reference
v^r_{sqHF} : q-axis HF voltage in the rotor reference
i^r_{sdHF} : d-axis HF current in the rotor reference
i^r_{sqHF} : q-axis HF current in the rotor reference
L_{dHF} : d-axis HF inductance
L_{qHF} : q-axis HF inductance
p : Differential operator. Equivalent to the s variable in Laplace transform.

If a rotating HF voltage signal is injected into the stator terminal of the machine (10), the HF currents induced in the stator windings are given by (11) and (12).

$$v^{r*}_{sdqHF} = V^*_{HF} e^{j(\omega_{HF} t)} = \begin{bmatrix} \bar{V}^{r*}_{sdHF} \\ \bar{V}^{r*}_{sqHF} \end{bmatrix} = \begin{bmatrix} V^*_{HF}\, cos\,(\omega_{HF} t) \\ V^*_{HF}\, sin\,(\omega_{HF} t) \end{bmatrix} \tag{10}$$

$$i^r_{sdHF} = \frac{R_{qHF} + j\omega_{HF} L_{qHF}}{(R_{dHF} + j\omega_{HF} L_{dHF})(R_{qHF} + j\omega_{HF} L_{qHF}) + \omega_r^2 L_{dHF} L_{qHF}} \cdot \left[v^{r*}_{sdHF} + \frac{\omega_r L_{qHF} v^{r*}_{sqHF}}{R_{qHF} + j\omega_{HF} L_{qHF}} \right] \tag{11}$$

$$i^r_{sqHF} = \frac{R_{dHF} + j\omega_{HF} L_{dHF}}{(R_{dHF} + j\omega_{HF} L_{dHF})(R_{qHF} + j\omega_{HF} L_{qHF}) + \omega_r^2 L_{dHF} L_{qHF}} \cdot \left[v^{r*}_{sqHF} - \frac{\omega_r L_{dHF} v^{r*}_{sdHF}}{R_{dHF} + j\omega_{HF} L_{dHF}} \right] \tag{12}$$

It can be seen from (11)-(12) that modeling of L_{dHF} and L_{qHF} is not straightforward due to cross-coupling between d and q axes and fundamental-speed dependent terms. However, if the frequency of the injected HF signal is sufficiently higher than the rotor frequency, the rotor speed dependent terms can be safely neglected, the HF currents induced in the stator can be therefore simplified to (13)-(14). An orientative value for this assumption can be $\omega_{HF} \geq \omega_r + 2\pi 500 rad/s$ [44].

$$i^r_{sdHF} = \frac{v^{r*}_{sdHF}}{(R_{dHF} + j\omega_{HF} L_{dHF})} \tag{13}$$

$$i^r_{sqHF} = \frac{v^{r*}_{sqHF}}{(R_{qHF} + j\omega_{HF} L_{qHF})} \tag{14}$$

Estimation of L_{dHF} and L_{qHF} can be finally obtained from the imaginary part of the dq HF impedance (15)-(18).

$$Z_{dHF} = R_{dHF} + j\omega_{HF} L_{dHF} = \frac{v^{r*}_{sdHF}}{i^r_{sdHF}} \tag{15}$$

$$Z_{qHF} = R_{qHF} + j\omega_{HF} L_{qHF} = \frac{v^{r*}_{sqHF}}{i^r_{sqHF}} \tag{16}$$

$$L_{dHF} = \frac{\Im(Z_{dHF})}{\omega_{HF}} \tag{17}$$

$$L_{qHF} = \frac{\Im(Z_{qHF})}{\omega_{HF}} \tag{18}$$

IV. Torque Estimation using dq HF inductances

The previous section has shown that real-time HF inductances estimation is possible from the machine response to a HF signal. It is important to notice however that HF inductances are not the inductances in the GTE.

As seen in section II, inductances in the GTE are the apparent inductances, which are given by the static permeability, μ_s (5) [see Fig. 1]. Therefore this definition only applies for the case of a static magnetic field (i.e. constant) excitation.

However, if a small HF alternating (AC) magnetic field is superposed on the static magnetic field, a minor hysteresis loop will be produced. The associated incremental permeability μ_Δ, is defined as (19) [49], [50].

$$\mu_\Delta = \frac{\Delta B}{\Delta H} \tag{19}$$

The area of the hysteresis loop will depend on the magnitude of the HF signal being injected. Assumed that the magnitude of the HF signal is small, the trajectory followed in the hysteresis loop can be approximated by a straight line [see Fig. 1]. This line will be tangent to the HB curve at the H-B coordinates corresponding to the DC excitation. In this case, the incremental permeability μ_Δ, can be approximated to the differential permeability μ_d, defined by (20) [49]–[51].

$$\mu_d = \frac{dB}{dH} \approx \mu_\Delta \tag{20}$$

Therefore, the term inductance may be defined in different ways with respect to the BH curve of the ferromagnetic materials and the injection and measured variables [49], [50]. This is discussed in the following subsection.

A. Apparent and Synchronous Inductance Definition

From the earlier discussion, the apparent inductances and the incremental can be defined as follows:

- The apparent (or synchronous) inductance governs the steady state behaviour of the electrical machine. This inductance is given by the static permeability (5) and can be graphically represented as the slope of the linearized characteristic of flux linkage versus current through the origin and the operating point of the magnetizing curve [see Fig. 2].

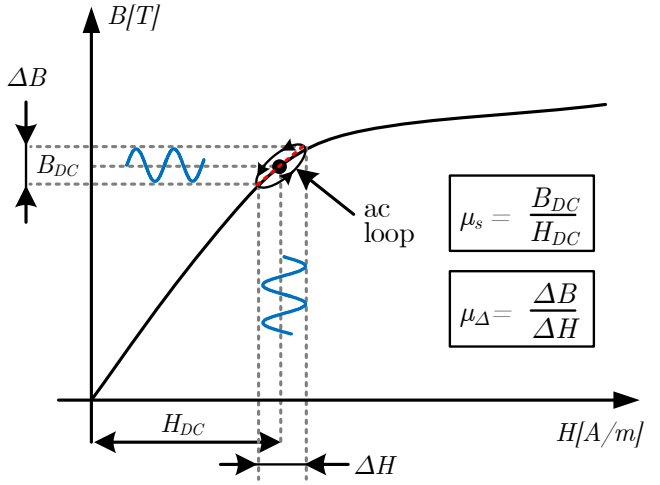

Fig. 1. Typical BH curve of a ferromagnetic material: static, incremental and differential permeability definition.

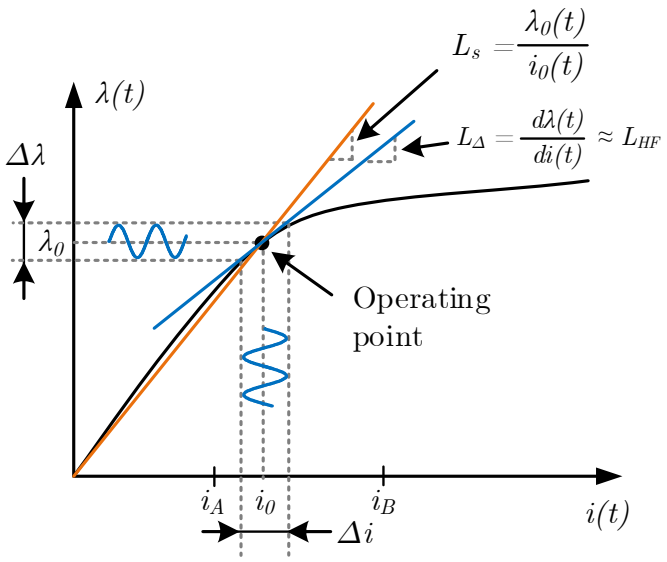

Fig. 2. Definition of the incremental and synchronous inductance.

$$L_s = \frac{\lambda(t)}{i(t)} \tag{21}$$

- The incremental (or differential) inductance governs the transient behaviour of electrical machines. The incremental inductances are given by the differential permeability (20) and can be graphically represented as the slope of the tangential line at the operating point of the magnetizing curve, as shown in Fig. 2. As a result, the dq-axes HF inductances, L_{dHF},L_{qHF} estimated using the proposed method (17)-(18) can be assumed to be equal to the differential inductance.

$$L_\Delta = \frac{d\lambda(t)}{di(t)} \approx L_{HF} \tag{22}$$

Figure 3 shows the corresponding synchronous and incremental inductances for the magnetizing curve shown in Fig. 2. It is seen from Fig. 3 that HF inductance could be assumed to be approximately equal to the synchronous inductances at low excitation levels (i.e linear region ($0 \leq i < i_A$)). However, once the machine starts to saturate (i.e. knee at $i \approx i_A$), a linear relationship between synchronous and HF inductances cannot be assumed anymore.

From the relationship between (21) and (22), it can be concluded that for current levels $> i_A$, the synchronous inductance can be directly estimated from the estimated HF inductances as follows:

$$\hat{L}_s(i) = \frac{\int_{0^+}^{i} L_{HF}\ di}{i} \tag{23}$$

It is noted that (23) only applies when the fundamental current is > 0. However, when fundamental current equals to 0A, L_{HF}=L_s holds [see Fig 3] and, additionally no torque would be produced. Therefore, using (23) will be necessary to guarantee accurate torque estimation at any torque level >0.

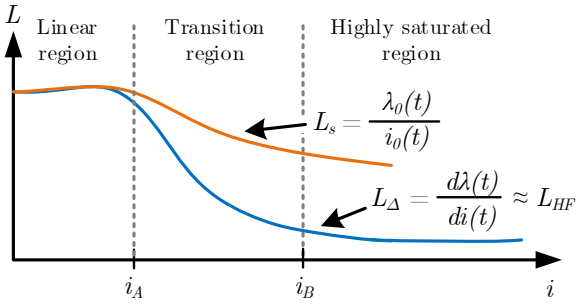

Fig. 3. Incremental and synchronous inductances of Fig. 2.

Particularizing (23) for d and q-axis and substituting it into the GTE, torque can be finally estimated as:

$$\hat{T}_e = \frac{3P}{2}\left[\left(\frac{\int_{0^+}^{i} L_{dHF(I_{sd},I_{sq})}\ di^r_{sd}}{i^r_{sd}} - \frac{\int_{0^+}^{i} L_{qHF(I_{sd},I_{sq})}\ di^r_{sq}}{i^r_{sq}}\right) i^r_{sd} i^r_{sq}\right] \tag{24}$$

Note that cross-coupling terms have not been taken into account. Also note that all the preceding discussions does not introduce any restriction to the signals feeding the machine, other than being high-frequency. Therefore, it applies to any form of HF excitation.

V. Simulation Results

This section shows simulation results of the proposed method obtained by means of Finite Element Analysis (FEA). Figure 4 shows the schematic representation of the machine that will be used both for simulation and experimental verification, the parameters being shown in Table I. It corresponds to

a commercial 4p SynRM [54]. L_{d0} and L_{q0} shown in table I have been measured using the procedure described in [55]. Figures 5 and 6 show simulations results changing both dq-axes fundamental currents from 0A to 3.9A (1 p.u.), with the machine rotating at rated speed (1500 r.p.m).

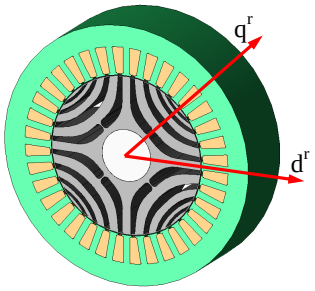

Fig. 4. Schematic representation of the 4-pole SynRM test machine.

Figures 5(a) and 5(b) show the measured d and q-axes magnetic fluxes. Figures 5(c) and 5(d) show the estimated synchronous, L_{dDC} and L_{qDC}, and HF , L_{dHF} and L_{qHF}, inductances using (21)-(22). It can be observed that once the machine starts to saturate, the HF inductance cannot be assumed to be equal to the synchronous inductance anymore [see Fig. 3]. This is an expected result, as the estimated HF inductances (22) are defined by the differential permeability (20).

Figures 5(e) and 5(f) show the estimated dq-axes DC inductances, $\hat{L}_{d_{DC}}$ and $\hat{L}_{d_{DC}}$, obtained by integration of the HF inductances shown in 5(c) and 5(d), using (23). Figures 5(g) and 5(g) show the estimation error. It is seen that synchronous inductances can be accurately estimated from the response to the injected HF signal even at high saturation level.

Figures 6(a) and 6(b) show the actual torque provided by FEA (T_{meas}), the estimated torque using the GTE assuming constant inductances ($\hat{T}_{L_{dq_0}}$) and the estimated torque using the estimated DC inductances shown in Figs. 5(e) and 5(f) ($\hat{T}_{\hat{L}_{dqDC}}$). Figs. 6(c) and 6(d) show the torque estimation errors defined as $T_{meas} - \hat{T}_{L_{dq_0}}$ and $T_{meas} - \hat{T}_{\hat{L}_{dqDC}}$. It can be observed that torque estimations using the proposed method significantly improve the accuracy especially for large values of dq-axes current, i.e. when the machine is highly saturated. It is observed that the maximum torque estimation error using the GTE with constant inductances is <3.3Nm ($\approx 34\%$ of rated torque), being reduced to <0.16 Nm ($\approx 1.7\%$ of rated torque) when DC inductances are estimated using the HF inductances.

TABLE I
MACHINE PARAMETERS

Rated torque	T_{rated}	9.55 Nm
Rated speed	n_{rated}	1500 rpm
Rated current	I_{rated}	3.9 A_{rms}
Poles pairs	P	2
d-axis inductance	L_{d0}	450 mH
q-axis inductance	L_{q0}	250 mH

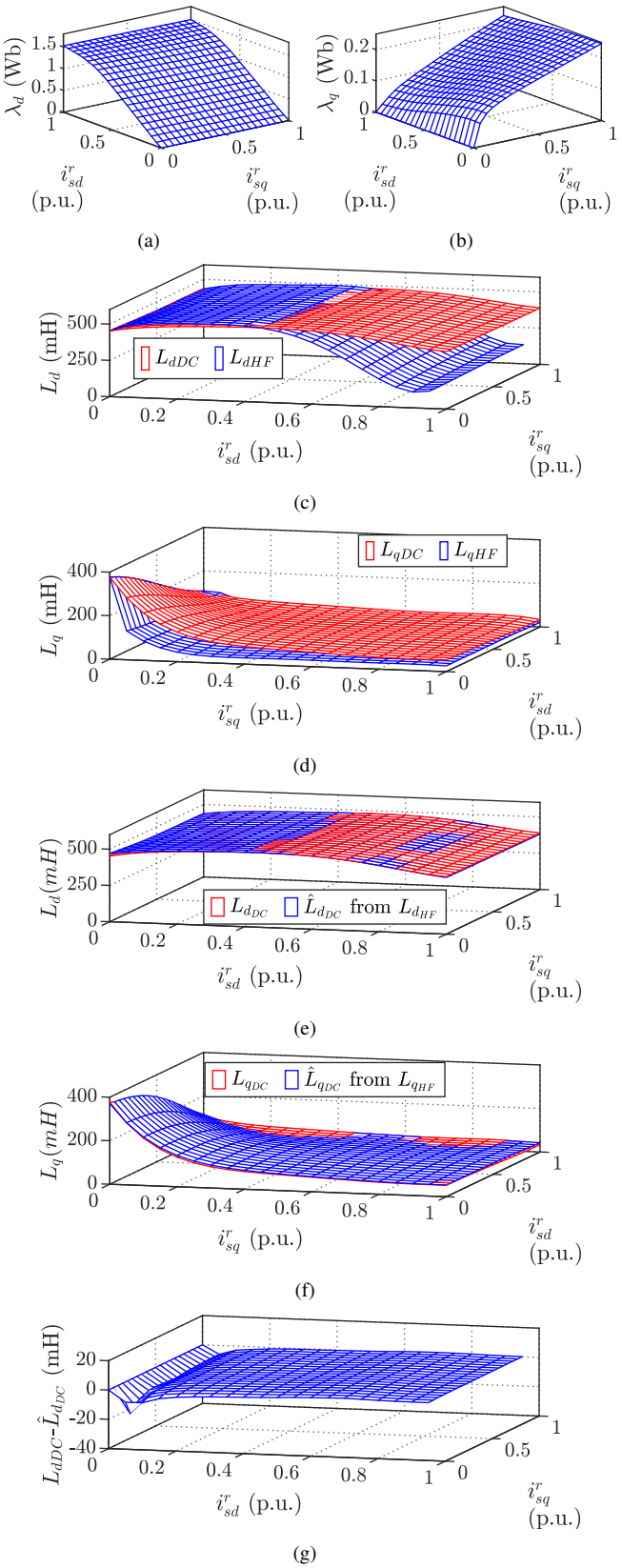

VI. Experimental Results

Experimental results have been conduced in a test bench consisting of the test machine [54], a load machine (1.85kW

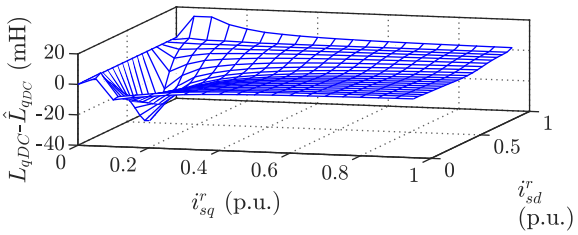

(h)

Fig. 5. FEA simulation results: (a) Measured d-axis flux; (b) Measured q-axis flux; (c) DC and HF d-axis inductances [see (21)-(22)]; (d) DC and HF q-axis inductances [see 21-22]; (e) DC and estimated DC d-axis inductances [see (21), (23)]; (f) DC and estimated DC q-axis inductances [see (21), (23)]; (g) d-axis synchronous inductance estimation error; (h) q-axis synchronous inductance estimation error.

IM) [56] and a torque sensor [57], which is used to assess the accuracy of the proposed method. Figure 7 shows the experimental setup. Details of the experimental setup parameters are summarized in Table II.

Figure 8(a) shows the inverter control block diagram while Fig. 8(b) shows the signal processing for torque estimation using a rotating HF voltage signal injection.

Inputs of the signal processing block are the commanded HF voltage v^{r*}_{sdqHF}, the induced HF currents i^r_{sdqHF}, and the fundamental commanded current i^{r*}_{sdq}. Figure 9(a) and Fig. 9(b) show the commanded dq-axes HF voltage and the corresponding FFT. A HF voltage of 40V and 500Hz has been used for all the experimental results. Figure 9(c) and Fig. 9(d) show the resulting stator dq-axes HF currents and the corresponding FFT. A discrete High Pass Filter (HPF) of 5Hz bandwidth has been used to remove the fundamental current component from the measured stator currents. Figures 9(e) and 9(f) show the dq-axes measured fundamental currents and the corresponding FFT after decoupling the induced HF currents and when the test machine is operated at its rated current. A discrete second-order low-pass filter (LPF) with a bandwidth of 100Hz has been used to remove the HF current from the measured current.

Dq-axes HF inductances are estimated from the HF voltages and currents shown in Fig. 9(a) and Fig. 9(c) using (17)-(18) [see Fig. 9(g)]. The synchronous inductances $\hat{L}_{dDC}$ and $\hat{L}_{qDC}$

TABLE II
EXPERIMENTAL TEST CONDITIONS

Power converter switching frequency, f_s	10kHz
Fundamental rotational speed, n_r	600 r.p.m.
High-frequency voltage magnitude, V_{HF}	40V
Frequency of the injected HF signal, ω_{HF}	2·π· 500 rad/ s
Low-Pass Filter bandwidth, bw_{LPF}	2·π· 100 rad/s
High-Pass Filter bandwidth, bw_{HPF}	2·π· 5 rad/s
Torque transducer measurement range [57]	±50Nm
Torque transducer combined error* [57]	<0.50%
Encoder resolution	4096
Accuracy Hall-effect based-current sensors	1%

*According to the calibrating curve provided by the manufacturer

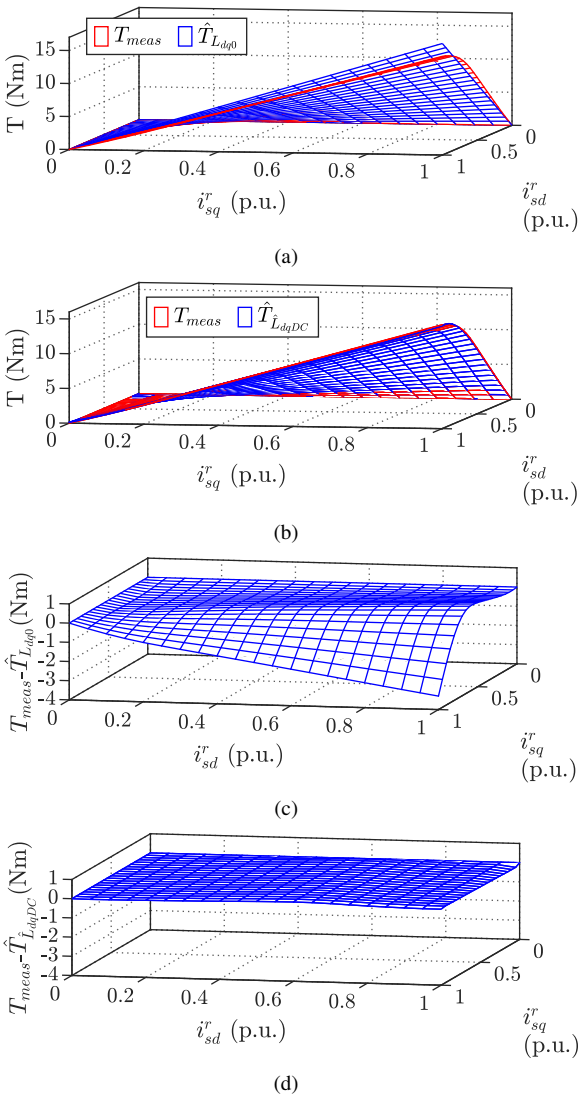

Fig. 6. FEA simulation results: (a) Measured and estimated torque assuming constant machine parameters; (b) Measured and estimated torque when DC inductances are estimated using the HF inductances; (c) Torque estimation error assuming constant machine parameters; (d) Torque estimated error from estimated DC parameters.

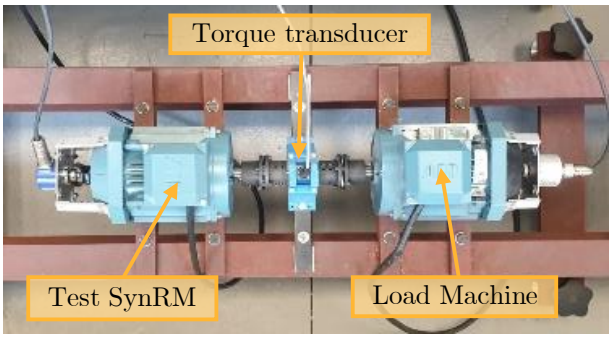

Fig. 7. Experimental set-up: Picture of the test bench.

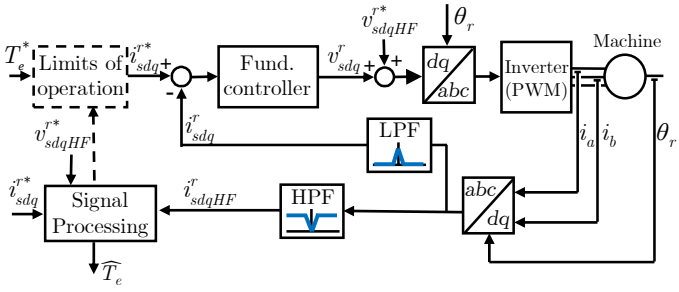

(a)

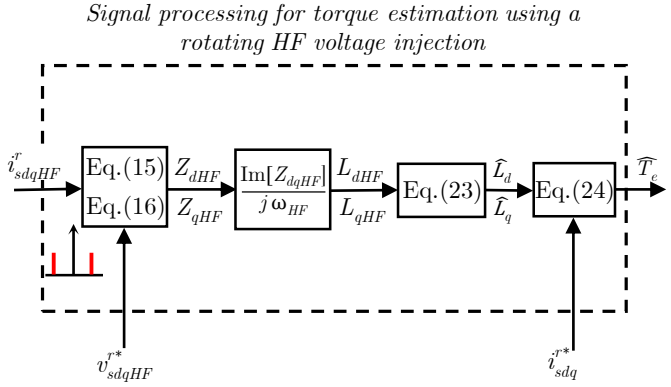

(b)

Fig. 8. Implementation of torque estimation using rotating HF voltage injection: (a) Power converter and control overview; (b) Signal processing.

are obtained using (23) [see Fig. 9(h)], torque estimation $\hat{T}_e$ being finally obtained using (24). Figure 9(i) shows the measured torque using the torque transducer (T_{meas}), the estimated torque using (4) (GTE) assuming constant inductances ($\hat{T}_{L_{dq_0}}$) and the estimated torque using the estimated DC inductances in Fig. 9(h) ($\hat{T}_{\hat{L}_{dqDC}}$). Finally, Fig. 9(j) shows the estimation errors.

Figure 10 shows the actual and estimated torque using the proposed method (24) when there is a step-like change in the dq-axes current command, i^{r*}_{sdq}, from 0.6 to 1 p.u. with a current angle $\beta = 45°$. (i.e.: dq-axes HF and synchronous inductances have been estimated from 0 to 0.6p.u. current level in steps of 0.05p.u. following the procedure described in Fig. 9 before applying the step-like change). It can be observed from the error shown in Fig. 10(b) that the torque estimator responds in the range of ms.

Figure 11 shows experimental results when the dq-axes fundamental currents, i^{r*}_{sd} and i^{r*}_{sq}, changes from 0 to 1p.u. in steps of 0.05p.u., and the machine rotates at 0.4p.u. (600rpm). It is noted that according to (23), the smaller the current steps, the better the resolution of synchronous inductance estimation,being the step size critical when the machine enters in the transition region [see Fig. 1]. The current step size has been chosen to accurately estimate both dq-axes inductances when the machine enters in the saturation region [see Fig. 5(a) and 5(b)].

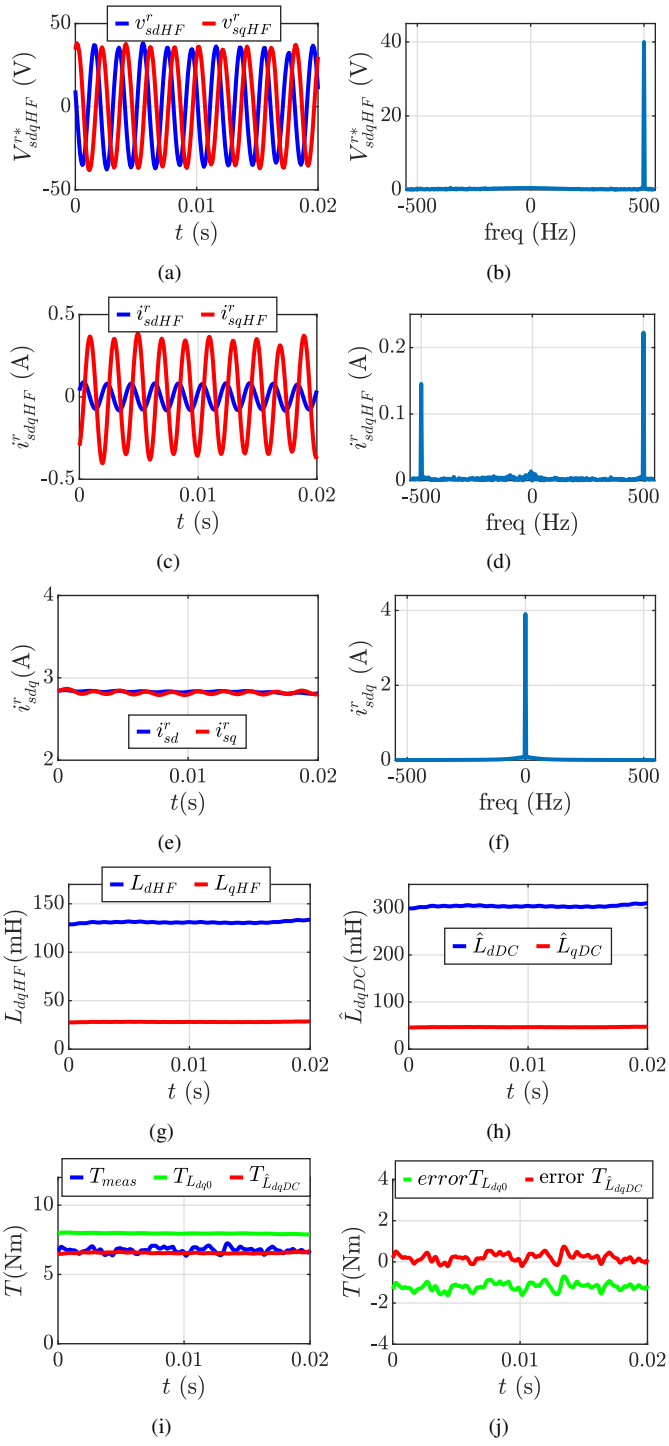

Fig. 9. Experimental results: (a) Injected HF voltage, v^{r*}_{sdqHF}; (b) FFT of v^{r*}_{sdqHF}; (c) Induced HF currents, i^{r}_{sdqHF}; (d) FFT of i^{r}_{sdqHF}; (e) Fundamental measured currents, i^{r}_{sdq}; (f) FFT of i^{r}_{sdq}; (g) Estimated dq-axes HF inductances [see (17)-(18)]; (h) Estimated DC synchronous inductances (23); (i) Estimated and measured torque; (j) Estimation errors, $T_{meas} - \hat{T}_{L_{dq_0}}$ and $T_{meas} - \hat{T}_{\hat{L}_{dqDC}}$. i^{r*}_{sdq}=1p.u. ω_r=0.4 p.u.

Figures 11(a) and 11(b) show the estimated d and q-axes HF inductances, L_{dHF} and L_{qHF} using (17)-(18) and the

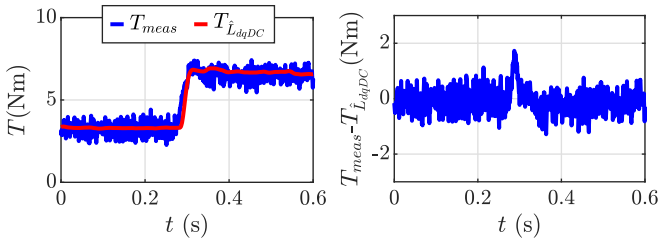

(a) (b)

Fig. 10. Experimental results: (a) Estimated and measured torque; (b) Estimated torque error. Transient response to a step-like change in dq-axes current command, i^{r*}_{sdq}, from 0.6 to 1p.u., with a current angle, β, of 45°. ω_r=0.4 p.u.

estimated synchronous inductances, $\hat{L}_{dDC}$ and $\hat{L}_{qDC}$ applying (23). Figures 11(c) and 11(e) show the measured torque using the torque transducer (T_{meas}), the estimated torque using (4) (GTE) assuming constant inductances ($\hat{T}_{L_{dq_0}}$) and the estimated torque from the estimated DC inductances in Fig. 11(a) and 11(b) ($\hat{T}_{\hat{L}_{dqDC}}$).

Figure 11(e) and 11(f) show the torque estimation errors. Error are seen to significantly decrease using the proposed method (24), specially in the high-saturation region. It is observed that the maximum toque estimation error when using the GTE assuming constant inductances is <3.15Nm (i.e. <33% of the rated torque of the machine), while it is reduced to <0.38 Nm (i.e. <3.9% of the rated torque of the machine) when using the proposed method. These results are in good agreement with the simulation results shown in Fig. 6(c) and Fig. 6(d). Discrepancies between FEA simulations and experimental results should be expected due assembling tolerances and/or mismatches between real materials and modelled materials. It is observed that the maximum error using the proposed method (24) occurs when the machine operates outside the Maximum Torque Per Ampere (MTPA) region (i.e. when the fundamental current, i^r_{sdq}, has a current angle β different from 45° [see Fig. 11(f)]). This effect is a matter of ongoing research.

VII. Conclusions

This paper proposes a method to enhance SynRM torque estimation using GTE by means of online parameter estimation. It has been demonstrated that synchronous inductances in the GTE can be accurately obtained by integrating the estimated HF inductances along the fundamental current. The proposed method has been shown to reduce significantly the torque estimation error, especially under deep saturation. Appealing properties of the proposed method are its capability to operate in real time, under any speed and load condition, and without requiring a commissioning process. However, implementation of the proposed method in applications in which the machine operates in the saturation region for long periods of time can be especially challenging, as this reduces the opportunities of refreshing the estimates. Additionally, continuously estimation of the synchronous inductance would be required for having

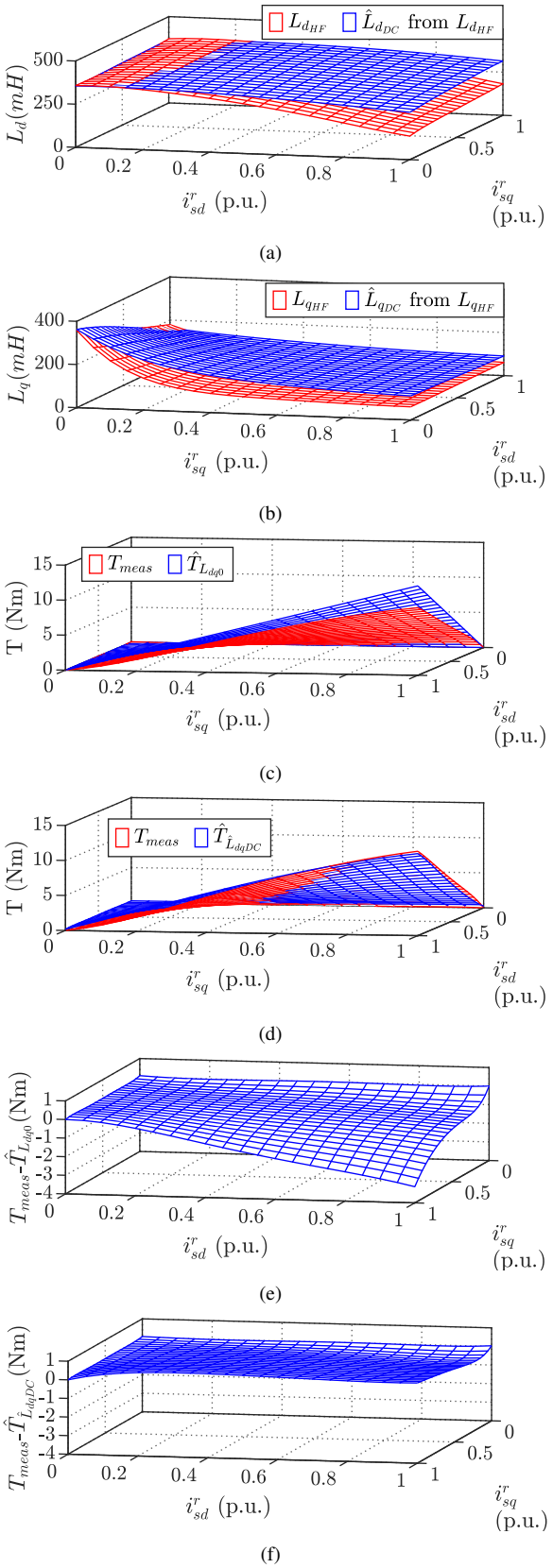

Fig. 11. Experimental results: (a) d-axis HF (17) and estimated DC inductances (23); (b) q-axis HF (18) and DC inductances (23); (c) Measured and estimated torque assuming constant machine parameters; (d) Measured and estimated torque when DC inductances are estimated using the HF inductances; (e) Torque estimation error assuming constant machine parameters; (f) Torque estimated error from estimated DC parameters.

a reduced torque estimation error, specially when the machine enters in the transition magnetic operating region.

REFERENCES

[1] A. Vagati, "The synchronous reluctance solution: a new alternative in ac drives," in *Proceedings of IECON'94 - 20th Annual Conference of IEEE Industrial Electronics*, vol. 1, 1994, pp. 1–13 vol.1.

[2] C. Babetto, G. Bacco, G. Berardi, and N. Bianchi, "High speed motors: A comparison between synchronous pm and reluctance machines," in *2017 IEEE Energy Conversion Congress and Exposition (ECCE)*, 2017, pp. 3927–3934.

[3] M. Zimmermann, A. Lange, and B. Piepenbreier, "Experimental results and parameter identification of a permanent magnet assisted synchronous reluctance machine with a ribless rotor," in *2018 IEEE International Magnetics Conference (INTERMAG)*, 2018, pp. 1–5.

[4] J. Malan and M. J. Kamper, "Performance of a hybrid electric vehicle using reluctance synchronous machine technology," *IEEE Transactions on Industry Applications*, vol. 37, no. 5, pp. 1319–1324, 2001.

[5] H. Huang, Y. Hu, Y. Xiao, and H. Lyu, "Research of parameters and antidemagnetization of rare-earth-less permanent magnet-assisted synchronous reluctance motor," *IEEE Transactions on Magnetics*, vol. 51, no. 11, pp. 1–4, 2015.

[6] T. Lubin, H. Razik, and A. Rezzoug, "Magnetic saturation effects on the control of a synchronous reluctance machine," *IEEE Transactions on Energy Conversion*, vol. 17, no. 3, pp. 356–362, 2002.

[7] T. Matsuo and T. A. Lipo, "Field oriented control of synchronous reluctance machine," in *IEEE Power Electronics Specialist Conference - PESC '93*, Jun. 1993, pp. 425–431.

[8] S. S. Maroufian and P. Pillay, "Torque characterization of a synchronous reluctance machine using an analytical model," *IEEE Transactions on Transportation Electrification*, vol. 4, no. 2, pp. 506–516, Jun. 2018.

[9] R. Shi, H. A. Toliyat, and A. El-Antably, "A dsp-based direct torque control of five-phase synchronous reluctance motor drive," in *IEEE Applied Power Electronics Conference and Exposition*, vol. 2, Mar. 2001, pp. 1077–1082.

[10] A. Shinke, M. Hasegawa, and K. Matsui, "Torque estimation for synchronous reluctance motors using robust flux observer to magnetic saturation," in *IEEE International Symposium on Industrial Electronics*, Jul. 2009, pp. 1569–1574.

[11] A. Yousefi-Talouki, P. Pescetto, G. Pellegrino, and I. Boldea, "Combined active flux and high-frequency injection methods for sensorless direct-flux vector control of synchronous reluctance machines," *IEEE Transactions on Power Electronics*, vol. 33, no. 3, pp. 2447–2457, Mar. 2018.

[12] Se-Kyo Chung, Hyun-Soo Kim, Chang-Gyun Kim, and Myung-Joong Youn, "A new instantaneous torque control of PM synchronous motor for high-performance direct-drive applications," *IEEE Transactions on Power Electronics*, vol. 13, no. 3, pp. 388–400, May 1998.

[13] S. Kim, J. Im, S. C. Go, J. Bae, W. Kim, K. Kim, C. Kim, and J. Lee, "Robust torque control of dc link voltage fluctuation for synrm considering inductances with magnetic saturation," *in IEEE Transactions on Magnetics*, vol. 46, no. 6, pp. 2005–2008, Jun. 2010.

[14] G. Heins, M. Thiele, and T. Brown, "Accurate Torque Ripple Measurement for PMSM," *IEEE Transactions on Instrumentation and Measurement*, vol. 60, no. 12, pp. 3868–3874, Dec. 2011.

[15] Interface. Torque sensors: T5, 2019. https://interfaceforce.co.uk/ , accessed 1-September-2019.

[16] HBM. HBM torque sensors. Available at https://www.hbm.com/en/0264/torque-transducers-torque-sensorstorque-meters/, accessed 16-October-2019.

[17] Futek. Futek torque sensors. Available at https://www.futek.com/store/Torque%20Sensors, accessed 16-October-2019.

[18] Magtrol motors testing and sensors. Magtrol torque transducers. Available at https://www.magtrol.com/product-category/torque-transducers/, accessed 16-October-2019.

[19] TE Connectivity. Measure Reaction and Rotating Torque. https://www.te.com/global-en/products/sensors/torque-sensors.html, accessed 16-October-2019.

[20] M. Martinez, D. Fernandez, D. Reigosa, J. M. Guerrero, and F. Briz, "Wireless torque pulsations measurement system for pmsms," 2020, pp. 1–1.

[21] P. Sue, D. Wilson, L. Farr, and A. Kretschmar, "High precision torque measurement on a rotating load coupling for power generation operations," in *IEEE International Instrumentation and Measurement Technology Conference Proceedings*, May 2012, pp. 518–523.

[22] J. Zakrzewski, "Combined magnetoelastic transducer for torque and force measurement," *IEEE Transactions on Instrumentation and Measurement*, vol. 46, no. 4, pp. 807–810, Aug. 1997.

[23] W. F. Traoré and R. McCann, "Torque measurements in synchronous generators using giant magnetoresistive sensor arrays via the Maxwell stress tensor," in *IEEE Power Energy Society General Meeting*, Jul. 2013, pp. 1–5.

[24] K. C. Yeo, G. Heins, and F. D. Boer, "Comparison of torque estimators for PMSM," in *in Australasian Universities Power Engineering Conference*, Dec. 2008, pp. 1–6.

[25] B. Cheng and T. R. Tesch, "Torque Feedforward Control Technique for Permanent-Magnet Synchronous Motors," *IEEE Transactions on Industrial Electronics*, vol. 57, no. 3, pp. 969–974, Mar. 2010.

[26] F. Jukic, D. Sumina, and I. Erceg, "Comparison of torque estimation methods for interior permanent magnet wind power generator," in *IEEE International Conference on Electrical Drives and Power Electronics (EDPE)*, Oct. 2017, pp. 291–296.

[27] J. X. Xu, S. K. Panda, Y. J. Pan, T. H. Lee, and B. H. Lam, "Improved PMSM pulsating torque minimization with iterative learning and sliding mode observer," in *IEEE International Conference on Industrial Electronics, Control and Instrumentation.*, vol. 3, Oct. 2000, pp. 1931–1936.

[28] B. H. Lam, S. K. Panda, and J. X. Xu, "Torque ripple minimization in PM synchronous motors an iterative learning control approach," in *IEEE International Conference on Power Electronics and Drive Systems. PEDS'99*, vol. 1, Jul. 1999, pp. 144–149 vol.1.

[29] X. Dong, W. Tianmiao, and W. Hongxing, "Comparison between model reference observer and reduced order observer of PMSM torque," in *IEEE Conference on Industrial Electronics and Applications*, Jun. 2011, pp. 663–667.

[30] Q. Liu and K. Hameyer, "High-Performance Adaptive Torque Control for an IPMSM With Real-Time MTPA Operation," *IEEE Transactions on Energy Conversion*, vol. 32, no. 2, pp. 571–581, Jun. 2017.

[31] Y. A.-I. Mohamed and T. K. Lee, "Adaptive self-tuning MTPA vector controller for IPMSM drive system," *IEEE Transactions on Energy Conversion*, vol. 21, no. 3, pp. 636–644, Sep. 2006.

[32] Atsushi Shinke, M. Hasegawa, and K. Matsui, "Torque estimation for synchronous reluctance motors using robust flux observer to magnetic saturation," in *IEEE International Symposium on Industrial Electronics*, Jul. 2009, pp. 1569–1574.

[33] P. L. Jansen and R. D. Lorenz, "A physically insightful approach to the design and accuracy assessment of flux observers for field oriented induction machine drives," *IEEE Transactions on Industry Applications*, vol. 30, no. 1, pp. 101–110, Jan. 1994.

[34] O. Buchholz and J. Böcker, "Gopinath-observer for flux estimation of an induction machine drive system," in *IEEE Southern Power Electronics Conference (SPEC)*, Dec. 2017, pp. 1–7.

[35] K.-H. Zhao, C.-F. Zhang, J. He, X.-F. Li, J.-H. Feng, J.-H. Liu, and T. Li, "Accurate torque-sensorless control approach for interior permanent-magnet synchronous machine based on cascaded sliding mode observer," *The Journal of Engineering*, vol. 2017, no. 7, pp. 376–384, 2017.

[36] G.-D. Andreescu, C. I. Pitic, F. Blaabjerg, and I. Boldea, "Combined Flux Observer With Signal Injection Enhancement for Wide Speed Range Sensorless Direct Torque Control of IPMSM Drives," *IEEE Transactions on Energy Conversion*, vol. 23, no. 2, pp. 393–402, Jun. 2008.

[37] X. Xiao, C. Chen, and M. Zhang, "Dynamic Permanent Magnet Flux Estimation of Permanent Magnet Synchronous Machines," *IEEE Transactions on Applied Superconductivity*, vol. 20, no. 3, pp. 1085–1088, Jun. 2010.

[38] K. Liu and Z. Q. Zhu, "Online Estimation of the Rotor Flux Linkage and Voltage-Source Inverter Nonlinearity in Permanent Magnet Synchronous Machine Drives," *IEEE Transactions on Power Electronics*, vol. 29, no. 1, pp. 418–427, Jan. 2014.

[39] M. N. Uddin, "An Adaptive-Filter-Based Torque-Ripple Minimization of a Fuzzy-Logic Controller for Speed Control of IPM Motor Drives," *IEEE Transactions on Industry Applications*, vol. 47, no. 1, pp. 350–358, Jan. 2011.

[40] T. Liu, I. Husain, and M. Elbuluk, "Torque ripple minimization with online parameter estimation using neural networks in permanent magnet

synchronous motors," in *IEEE Industry Applications Conference. Thirty-Third IAS Annual Meeting*, vol. 1, Oct. 1998, pp. 35–40 vol.1.

[41] Z. Lin, D. S. Reay, B. W. Williams, and X. He, "Online Modeling for Switched Reluctance Motors Using B-Spline Neural Networks," *IEEE Transactions on Industrial Electronics*, vol. 54, no. 6, pp. 3317–3322, Dec. 2007.

[42] W. Xu and R. D. Lorenz, "High-Frequency Injection-Based Stator Flux Linkage and Torque Estimation for DB-DTFC Implementation on IPMSMs Considering Cross-Saturation Effects," *IEEE Transactions on Industry Applications*, vol. 50, no. 6, pp. 3805–3815, Nov. 2014.

[43] B. Hafez, A. Abdel-Khalik, A. M. Massoud, S. Ahmed, and R. D. Lorenz, "Single sensor three-phase permanent magnet synchronous motor drive based on luenberger style-observers," in *15th IEEE International Conference on Electrical Machines and Systems (ICEMS)*, Oct. 2012, pp. 1–6.

[44] M. Martinez, D. Reigosa, D. Fernández, J. M. Guerrero, and F. Briz, "Enhancement of permanent-magnet synchronous machines torque estimation using pulsating high-frequency current injection," *IEEE Transactions on Industry Applications*, vol. 56, no. 1, pp. 358–366, Jan. 2020.

[45] D. Reigosa, D. Fernandez, T. Tanimoto, T. Kato, and F. Briz, "Comparative Analysis of BEMF and Pulsating High-Frequency Current Injection Methods for PM Temperature Estimation in PMSMs," *IEEE Transactions on Power Electronics*, vol. 32, no. 5, pp. 3691–3699, May 2017.

[46] Y. G. Kang, D. Reigosa, B. Sarlioglu, and R. D. Lorenz, "D- and q-axis inductance estimation and self-sensing condition monitoring using 45° angle high-frequency injection," *IEEE Transactions on Industry Applications*, vol. 57, no. 1, pp. 506–515, 2021.

[47] M. Martinez, D. F. Laborda, D. Reigosa, D. Fernández, J. M. Guerrero, and F. Briz, "Synrm sensorless torque estimation using high frequency signal injection," in *IEEE 10th International Symposium on Sensorless Control for Electrical Drives (SLED)*, Sep. 2019, pp. 1–5.

[48] M. Martinez, D. Reigosa, D. Fernandez, and F. Briz, "Comparative Analysis of High Frequency Signal Injection Based Torque Estimation Methods for SPMSM, IPMSM and SynRM," *Energies*, vol. 13, no. 3, p. 592, Jan. 2020. [Online]. Available: https://www.mdpi.com/1996-1073/13/3/592

[49] W. J. Croisant, C. A. Feickert, and M. K. McInerney, "A differential magnetic permeability model for pulsed magnetic field calculations," *IEEE Transactions on Magnetics*, vol. 32, no. 5, pp. 4326–4328, 1996.

[50] M. S. Perdigao, M. F. Menke, R. Seidel, R. A. Pinto, and J. M. Alonso, "A review on variable inductors and variable transformers: Applications to lighting drivers," *IEEE Transactions on Industry Applications*, vol. 52, no. 1, pp. 531–547, 2016.

[51] A. Ganji, P. Guillaume, R. Pintelon, and P. Lataire, "Induction motor dynamic and static inductance identification using a broadband excitation technique," *IEEE Transactions on Energy Conversion*, vol. 13, no. 1, pp. 15–20, Mar. 1998.

[52] D. D. Reigosa, D. Fernandez, H. Yoshida, T. Kato, and F. Briz, "Permanent-Magnet Temperature Estimation in PMSMs Using Pulsating High-Frequency Current Injection," *IEEE Transactions on Industry Applications*, vol. 51, no. 4, pp. 3159–3168, Jul. 2015.

[53] H. Jung, D. Park, H. Kim, S. Sul, and D. J. Berry, "Non-Invasive Magnet Temperature Estimation of IPMSM Based on High-Frequency Inductance With a Pulsating High-Frequency Voltage Signal Injection," *IEEE Transactions on Industry Applications*, vol. 55, no. 3, pp. 3076–3086, May 2019.

[54] ABB. ABB products: 3GAL092007-ASB. Available at https://new.abb.com/products/es/3GAL092007-ASB, accessed 15-December-2019.

[55] V. Bobek, "PMSM electrical parameters measurement," p. 16.

[56] ABB. ABB products: 3GAA092003-ASE. Available at https://new.abb.com/products/3GAA092003-ASE, accessed 15-December-2019.

[57] DELTA REGIS. Serie DRTX: DRTX-3138-50C. Available at https://deltaregis.com/, accessed 15-December-2019.